IEEE CGNCC 2014

August 8-10, 2014, Yantai, China

Program Digest

http://cgncc.buaa.edu.cn

IEEE CSS Chapter, Singapore

IEEE AESS Beijing Chapter

IEEE CSS Chapter, Nanjing, China

Situation for Dynamic Inverse Control Law

Sen Yang — Flight Automatic Control Research Institute
Xianglun Zhang — Flight Automatic Control Research Institute

14:00-14:15 SatA6.3

Compound Angle-Synchronizing Control Strategy for Dual Electro- Hydraulic Motors in HydraulicFlight Motion Simulator

Wenhao Dong — Beihang Univ.
Songshan Han — Beihang Univ.
Zongxia Jiao — Beihang Univ.
Shuai Wu — Beihang Univ.
Yifei Zhao — Beihang Univ.

14:15-14:30 SatA6.4

Adaptive Robust H∞Control for Uncertain Discrete-Time Systems with Time-Varying State and Input Delays

Cunwu Han — North China University of Technology
Fengmei Zhang — North China University of Technology
Lei Liu — North China University of Technology
Song Bi — North China University of Technology
Dehui Sun — North China University of Technology

14:30-14:45 SatA6.5

Internal Model Tracking Control of an Uncertain Impulsive Switched System

Jian Chen — Beihang Univ.
Chen Bai — Beihang Univ.
Qingdong Li — Beihang Univ.
Cunjia Liu — Loughborough Univ.
Yuan Tian — Beijing Institute of Space Long March Vehicle
Zhang Ren — Beihang Univ.

14:45-15:00 SatA6.6

Observer-based Control of One-sided Lipschitz Nonlinear Systems

Rui Wu — Shanghai University of Engineering Science
Wei Zhang — Shanghai University of Engineering Science
Jian Li — Shanghai University of Engineering Science
Zhiyang Wu — Shanghai University of Engineering Science

15:00-15:15 SatA6.7

Robust Attitude Control for Flexible Satellite During Orbit Maneuver

Long Li — Harbin Institute of Technology
Jing Yang — Harbin Institute of Technology
Xiaoping Shi — Harbin Institute of Technology
Hailong Liu — Harbin Institute of Technology

15:15-15:30 SatA6.8

Dynamic Control Algorithm Design of the 6 Wheel-drive All-terrain Robotic Skid-steered Vehicles

Tong Liu — Luoyang Institute of Electro-Optical Equipment, AVIC
Wei Li — Luoyang Institute of Electro-Optical Equipment, AVIC
Beile Wang — Luoyang Institute of Electro-Optical Equipment, AVIC
Yuqian Li — Luoyang Institute of Electro-Optical Equipment, AVIC

SatA7 APPHIRE
Modeling & Simulation I (Regular Session)

Chair: Junsheng You — Air Force Institute of Aeromedicine
Haijun Zhou — Xi'an Flight Automatic Control Research Institute

13:30-13:45 SatA7.1

Research on Modeling of Morphing Aircraft

Bowen Li — Xi'an Flight Automatic Control Research Institute
Haijun Zhou — Xi'an Flight Automatic Control Research Institute
Xianglun Zhang — Xi'an Flight Automatic Control Research Institute
Jun Che — Xi'an Flight Automatic Control Research Institute
Kepu Song — Xi'an Flight Automatic Control Research Institute

13:45-14:00 SatA7.2

Modeling and Modal Responses Analysis of an Unmanned Small-Scaled Gyroplane

Changle Xiang — Beijing Institute of Technology
Xiaoliang Wang — Beijing Institute of Technology
Yue Ma — Beijing Institute of Technology
Yang Wang — Beijing Institute of Technology

14:00-14:15 SatA7.3

An Optimization Method of Aircraft Periodic Inspection and Maintenance Based on the Zero-Failure Data Analysis

Jun Huang — Naval Aeronautical and Astronautical Univ.
Yanbo Song — Naval Aeronautical and Astronautical Univ.
Yongji Ren — Naval Aeronautical and Astronautical Univ.
Qingwei Gao — Naval Aeronautical and Astronautical Univ.

14:15-14:30 SatA7.4

Background Modeling in Infrared Guidance Hardware-in-loop Simulation System

Haowen Zhang — Beihang Univ.
Wulong Zhang — Beijing Simulation Center
Yunjie Wu — Beihang Univ.
Jianmin Wang — Beihang Univ.

14:30-14:45 SatA7.5

Research on Boundary Layer Ingestion Effects of Distributed Propulsion Configuration

Wenwen Kang — Beihang Univ.
Jing Zhang — Beihang Univ.
Lingyu Yang — Beihang Univ.

14:45-15:00 SatA7.6

Research on Supercirculation Effects of Distributed Propulsion Configuration

Wenwen Kang — Beihang Univ.
Jing Zhang — Beihang Univ.
Lingyu Yang — Beihang Univ.

15:00-15:15 SatA7.7

An HLA/RTI Architecture Based on Periodic and Aperiodic Tasks Scheduling for Real-time Improvement

Shutian Liu — Beihang Univ.
Shuling Dai — Beihang Univ.

15:15-15:30 SatA7.8

A Real-Time Flight Simulation System Based on Rapid Prototyping and VxWorks

Xintao Liao — Nanjing Univ. of Aeronautics and Astronautics

Research on Supercirculation Effects of Distributed Propulsion Configuration

Wenwen Kang, Jing Zhang, Lingyu Yang

***Abstract*—this paper presents a systematic research on the supercirculation effects of Distributed Propulsion Configuration, based on a mathematical model of the distributed propulsion system and a sliced CFD model of SAX-40. Multiple factors which can affect supercirculation effects such as the deflection angle of thrust, Boundary Layer Ingestion effects, jet flow velocity, Angle of Attack and flight speed are examined. The influence regularities of supercirculation on aerodynamic parameters are summarized. Computation results indicate that the supercirculation effects have extraordinary potential to raise Cl and L/D ratio, thus resulting in a better flight performance; but due to the complexity of the influence regularities, there may be some difficulties in employing the supercirculation effects.**

I. INTRODUCTION

To realize Greener Aviation, the requirements proposed by NASA on the next generation of large civil aircraft are highly demanding, including pollution emission and noise level etc. The specifications of "N+X" program [1] are shown as Table 1:

Table 1 Requirements of "N+X" Program

Technical Objectives	Levels of Advanced Technology		
	N+1（2015） Compared to B737-800	N+2（2020） Compared to B777-200	N+3（2025） Compared to B737-800
Noise	-32dB	-42dB	-71dB
NOx emission during TO&L	-60%	-75%	-80%
NOx emission during Cruising	-55%	-70%	-80%
Fuel Consumption	-33%	-50%	-60%

To achieve these ambitious objectives, two configurations are being demonstrated ardently, and shown as Figure 1:

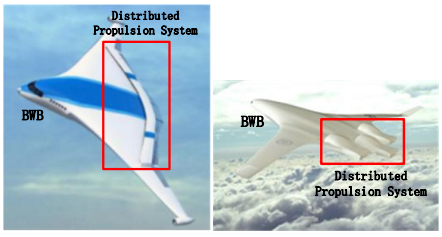

Figure 1 Configurations of "N+3" and SAX-40

*Resrach supported by the National Natural Science Foundation under grant #61304030.

F. A. Wenwen Kang is with the Science and Technology on Aircraft Control Laboratory, Beihang University, Beijing, 100191 China (e-mail: wanderkang0530@163.com).

S. B. Jing Zhang and S.C. Lingyu Yang is with School of Automation Science and Electrical Engineering, Beihang University, Beijing, 100191 China.(e-mail: jijizhj1982@163.com)

Their common features are the applications of BWB (Blended Wing Body) layout and Distributed Propulsion System (DPS), namely Distributed Propulsion Configuration (DPC). DPC is a new integrated design pattern of large civil aircraft, and it can reduce pollution emission and noise level on a large scale while increasing the fuel economy efficiency and range substantially.

Compared with traditional BWB aircraft, the most important innovation of DPC is the application of a semi-embedded DPS which employs two-dimensional nozzles featuring Thrust Vector (TV). The thrust vector can induce an intense supercirculation around the middle of fuselage and in consequence, the lift coefficient i.e. Cl and L/D ratio may be raised by a large margin. With the general use of supercritical airfoil in BWB layout design, the supercirculation effects can be effectively enhanced.

Current research on supercirculation can be divided into three categories, including power augmentation based on the Coanda Effect[2], jet flap[3] and thrust vector[4]; the methods applied to conduct the research includes wind tunnel experiments and CFD (Computational Fluid Dynamics) simulation. The reliability of wind tunnel experiments is relatively high, but it consumes too much resources and the environment factors considered in a wind tunnel experiment are limited; CFD simulation is quickly taking the duty to be a primary approach to conduct fluid dynamics research, and it is rapidly becoming more and more reliable, because: (1) its resource consuming level is low; (2) with the revolutionized enhancement of computing power and with the unceasing refinement of numerical algorithms, it is getting easier to solve the complex equations of fluid dynamics on a large scale.

Previous research on supercirculation is usually carried out by wind tunnel experiments, and only the influence of jet flow is considered, excluding the block effect of inlet. However, the most essential feature of DPC is the interference of the Boundary Layer Ingestion (BLI) effects and the supercirculation effects, which cannot be discussed separately. The focus of this paper is the supercirculation effects which are induced by thrust vector and affected by BLI effects. SAX-40, which is a typical represent of DPC and is demonstrated by the union of Cambridge University and MIT, is chosen as the research object, and CFD method is applied.

To simulate thrust vector and supercirculation effects effectively and with high fidelity, a mathematical model of DPS and a set of CFD models of SAX-40 are established firstly; then simulation under different conditions is carried out; finally the influence regularities of supercirculation effects on aerodynamic characteristics are summarized. The DPS model can provide inlet/outlet parameters of engine for

CFD model as boundary conditions, and provide other propulsion system states such as thrust and power etc. Simulation results of CFD model will be used to modify the DPS model, and support the analysis of supercirculation effects.

II. Definition of Supercirculation

By means of deflecting jet flow or generating jet flow on the surface around an airfoil, the parameter distribution of the flow field around the airfoil can be altered and the aerodynamic performance can be improved conspicuously by the inducing effects, which are called supercirculation. The supercirculation effects work like a flap, and it generally can be generated by three methods, including jet flow on the upper surface of airfoil, jet flap and thrust vector.

Jet flow on the upper surface is illustrated as Figure 2:

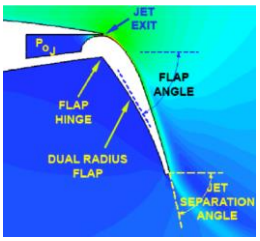

Figure 2 Jet Flow on the Upper Surface

Taking advantage of the Coanda Effect, which means the phenomenon of flowing adhered on walls, the decelerated air flow on the upper surface of airfoil due to friction is induced by the high-speed jet flow, and it will adhere to the large deflected flaps, resulting in delaying even eliminating the flow separation. In this way, the supercirculation can raise lift force substantially and effectively decrease the augmented pressure drag caused by the large deflection of flaps. Jet flow on the upper surface is the most widespread way to raise the L/D ratio, especially on large transport aircrafts, e.g. B747.

The jet flap and thrust vector can be classified into one category, because of the same enabling mechanism. These two situations are shown as Figure 3 and Figure 4:

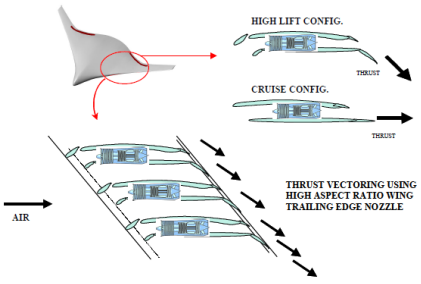

Figure 3 Jet Flap

Figure 4 Thrust vector

Via the direct alteration on the flow field behind the rear edge by high-speed jet flow, the inducing effect can change the air velocity distribution around the airfoil, and simultaneously change the pressure distribution. In consequence, the aerodynamic performance of the airfoil can be apparently improved. The 2D illustration of thrust vector is shown as Figure 5:

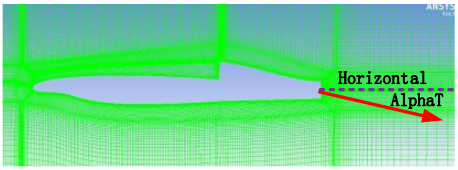

Figure 5 2D Illustration of Thrust vector

As is shown in the figure, the deflection angle of the jet flow relative to the horizontal is described as "*AlphaT*".

The wind tunnel experiment results by Langley Research center of NASA reveal that with regards to clean model, the deflection of thrust can induce a strong supercirculation. As a result of this, Cl will increase by a large margin; on the contrary the drag coefficient i.e. Cd will decrease under certain conditions. But for a DPC aircraft, due to the block of inlet and the BLI effects in front of the inlet, the supercirculation effects induced by the thrust vector may be more complex, which needs a systematic research.

III. Modeling of DPS and 2D sliced SAX-40

A. *Mathematical model of DPS*

The purpose of building a DPS mathematical model is to provide boundary conditions for the CFD model, and to calculate engine states data such as thrust. The DPS of SAX-40 consists of three sets of engines, and the adjustable parameters of each set are independent. The structure of SAX-40's DPS is shown as Figure 6:

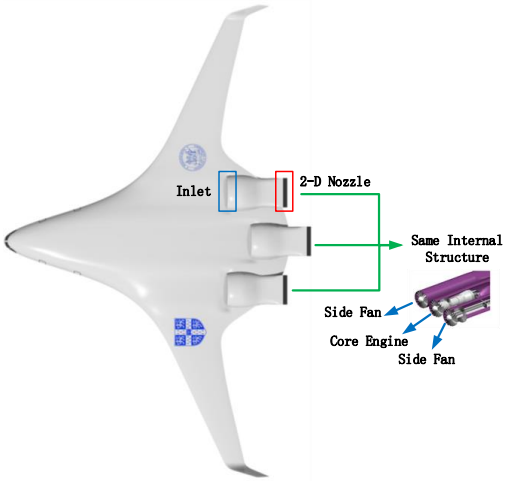

Figure 6 DPS of SAX-40

Each set of engines is combined with three separate fans, which are located in three separated tunnels, but the inlet and nozzle are common; the core engine is in the middle tunnel, and provides power to all three fans by gear mechanism.

To Simplify the DPS model, two assumptions are taken into consideration:

1) The impact of BLI on the engine is not considered, and the performance of three fans are assumed to be ideal;

2) The thermodynamic and gas dynamic parameters at inlet and outlet are the same as each tunnel.

One of the three sets of Simplified DPS model is shown as Figure 7:

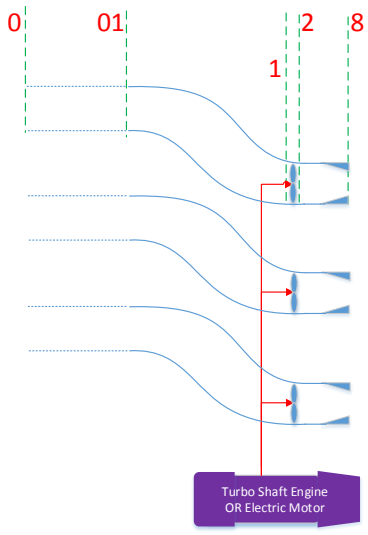

Figure 7 Illustration of DPS Model

Explanations of section number: "0"represents the entrance of selected control body, which is located in the undisturbed airflow far ahead; "01" represents the entrance of inlet; "1" represents the front section of fan; "2" represents the rear section of fan; "8" represents the exit of nozzle; area between "0" section and "01" section is called pre-compression segment; inlet is located between "01" section and "1" section; fan is located between "1" section and "2" section; nozzle is located between "2" section and "8" section.

The DPS model has three sets of engines or nine tunnels in total, and each tunnel has the same structure, thus only one tunnel is modeled. The detailed modeling process is shown as below:

1) Explanation of air conditions

Given the Mach number and altitude, the static pressure, static temperature, flight velocity P_0, T_0, V_0 and total pressure (i.e. stagnation pressure), total temperature, sound velocity, Mach number P_0^*, T_0^*, a_0, Ma_0 can be obtained.

The model is built according to the principle of constant specific heat, and the constant specific heat ratio is $\gamma = 1.4$; the gas constant of air is $R = 287.06(kg * K)$. Some important parameters can be described as functions of γ and R, shown as below:

a) the specific heat at constant pressure is $Cp = \frac{\gamma}{\gamma - 1} R$;

b) the coefficient of flow function is $K = \sqrt{\frac{\gamma}{R}\left(\frac{2}{\gamma+1}\right)^{\frac{\gamma+1}{\gamma-1}}}$;

c) the critical pressure ratio of nozzle is $\beta_{cr} = \frac{P_{ecr}}{P_e^*} = \left(\frac{2}{\gamma+1}\right)^{\frac{\gamma}{\gamma+1}}$;

d) the sound velocity of each point in the flow field is $a = \sqrt{\gamma RT}$.

2) Modeling of engine components

The thermodynamic process of each component is assumed as: (1) the pre-compression segment has an adiabatic process, which means the total temperature T^* and total pressure P^* in this segment are invariant; (2) the inlet also has an adiabatic process, but there is loss in total pressure, and the total pressure recovery coefficient σ_i is assumed as a constant; (3) the fan is a main power-consuming component in each tunnel, and its pressure ratio π_k^* is an adjustable parameter; (4) the nozzle is a convergent tube, and it has an adiabatic process. The area of its exit $A8$ can be adjusted. Similarly there is a loss in total pressure σ_e.

Adjustable parameters of each tunnel include fan pressure ratio π_k^* and nozzle outlet area $A8$.

Based on the above assumption of thermodynamic process of each component, characteristic equations can be summarized as below:

a) Pre-compression segment, $P_{01}^* = P_0^*, T_{01}^* = T_0^*$;

b) Inlet, $P_1^* = \sigma_i * P_{01}^*$, $T_1^* = T_{01}^*$;

c) Fan, $P_2^* = \pi_k^* * P_1^*$, $T_2^* = T_1^* * \left(\pi_k^*\right)^{\frac{\gamma-1}{\gamma}}$;

d) Nozzle, $P_8^* = \sigma_e * P_2^*, T_8^* = T_2^*$.

3) Balance of air mass flow rate at each section

The air mass flow rates at the inlet and outlet of each tunnel are the same, which can be described as:

$$q_m = K \frac{P_{01}^* * A_{01} * q(\lambda_{01})}{\sqrt{T_{01}^*}} = K \frac{P_8^* * A_8 * q(\lambda_8)}{\sqrt{T_8^*}} \quad (1)$$

Using the characteristic equations of components, equation as below can be deduced:

$$q(\lambda_{01}) = \sigma_i * \left(\pi_k^*\right)^{\frac{\gamma+1}{2\gamma}} * A_8 * q(\lambda_8) / A_{01} \quad (2)$$

4) Supplementary equations

Because A_8 is a critical section, the air condition at this section must be analyzed to determine whether the compressed air in the nozzle is fully expanded.

Total pressure P^* and static pressure P in the flow field has relationship as:

$$\frac{P^*}{P}=\left(1+\frac{\gamma-1}{2}Ma^2\right)^{\frac{\gamma}{\gamma-1}} \tag{3}$$

Total pressure T^* and static pressure T in the flow field has relationship as:

$$\frac{T^*}{T}=1+\frac{\gamma-1}{2}Ma^2 \tag{4}$$

5) Thrust and power

The air velocity at A_8 is $V_8=Ma_8*a_8=Ma_8*\sqrt{\gamma RT_8}$, therefore the thrust of each tunnel is:

$$F=q_m*(V_8-V_0)+A8*(P_8-P_0) \tag{5}$$

And the power-consumed of each tunnel is:

$$P_{re}=q_m*w_k \tag{6}$$

Where w_k is the power consumed by unit air mass flow rate, and it can be described as:

$$w_k=Cp(T_2^*-T_1^*)/\eta_k^*=\frac{\gamma}{\gamma-1}R*T_0^**\left[\left(\pi_k^*\right)^{\frac{\gamma-1}{\gamma}}-1\right]/\eta_k^* \tag{7}$$

In which, η_k^* is the efficiency of power transmission from shaft power to compression power.

As above, all the equations needed to build a DPS mathematical model are described. If the initial conditions are set, all the thermodynamic and gas dynamic parameters at each section can be obtained.

B. 2D sliced CFD model of SAX-40

The sliced model of SAX-40 is firstly conducted to explore BLI effects on 2-Dimension. Modeling of SAX-40 consists of two main procedures:

1) 3D clean CFD model of SAX-40 should be established to prove the validity of SAX-40 configuration. And the numerical simulation results prove that the configuration of SAX-40 is rational and can be regarded as the base line of further discussion. Due to the space limitation, the detailed process is omitted.

2) 2D sliced clean model should be extracted from 3D model, and the 2D model can be modified into an intact one with the integration of DPS model;

Apparently, supercirculation will affect the whole central fuselage, but only the regions shown as Figure 8 in shadows are considered in purpose of simplifying the analysis.

Since the 3D shape of SAX-40 has been established, 2D sliced model can be easily extracted from the corresponding position from 3D model. Taking the areas affected by supercirculation into consideration, Clean airfoil of "7" position is extracted, shown as Figure 9.

With the specific design parameters of DPS model, the 2D clean airfoil can be modified with the shape of propulsion system, and the modified results are shown as Figure 10.

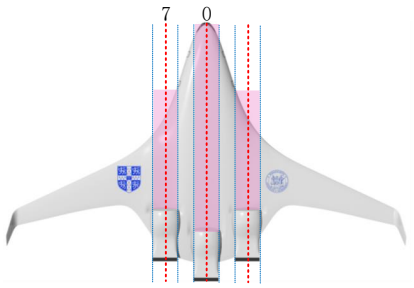

Figure 8 Effect Regions of Supercirculation

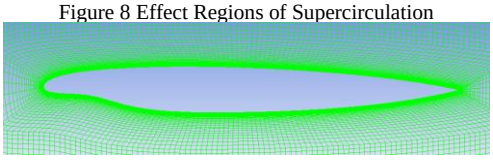

Figure 9 Clean Airfoils of "7" Slice and "0" Slice

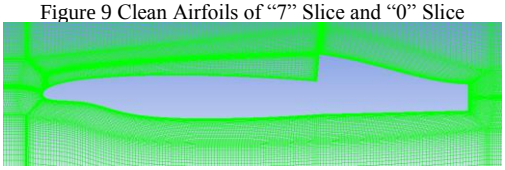

Figure 10 Airfoil with DPS model of Slice "7" and Slice "0"

To simulate supercirculation effects with CFD measures, the DPS model should be integrated into the CFD model. The DPS model provides the CFD model with boundary conditions, shown as Figure 11:

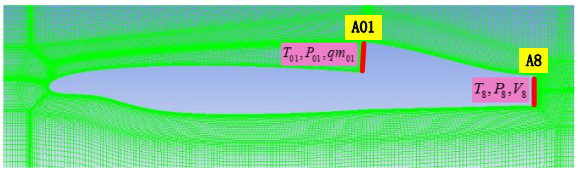

Figure 11 Boundary Conditions of CFD model

The thrust vector is illustrated as figure 5.

IV. STUDY ON INFLUENCE REGULARITIES OF SUPERCIRCULATION

As described before, the supercirculation effects may have strong influence on the aerodynamic performance of DPC aircraft. Multiple factors can affect the effectiveness of the supercirculation, including the deflection angle of thrust, BLI effects, jet velocity, AOA and flight speed, etc. To analyze conveniently, engineering approach named fixed-variable method is adopted and only one or two factors is considered each time.

The "7" slice in figure 8 is selected as the analysis area. The supercirculation effects of SAX-40 are analyzed and the influence regularities on aerodynamic performance are summarized. Two simulation conditions are chosen, shown as below:

1) $Ma=0.6, H=10000m$;

2) $Ma=0.8, H=10000m$.

The deflection angle of thrust is described as "AlphaT", and the downward deflection is defined as "negative"; the upward deflection is defined as "positive". The limited range of deflection is $AlphaT\in\left(-7^o,5^o\right)$.

A. *Influence of AlphaT on supercirculation*

AlphaT is the elemental factor to enable supercirculation. Under conditions of BLI intensity $\eta_{BLI} = 1.08$, jet velocity $V8 = 285.3m/s$, $AOA = 0^o$ and $Ma = 0.6$, the velocity nephograms under different thrust deflection angles including -7^o , 0^o and 5^o are shown as Figure 12:

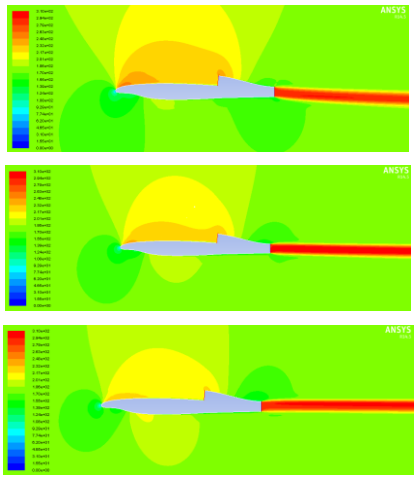

Figure 12 Velocity Nephograms of Thrust vector

An obvious phenomenon is that when the thrust deflects downward, the inducing effect on the upper surface flow field is strong, and the blocking effect on the under surface flow field is strong too. The alteration of velocity distribution will directly affect the pressure distribution, and the pressure nephograms responding to -7^o , 0^o and 5^o are shown as Figure 13.

As can be seen, along with the thrust deflection angle changing from negative to positive, the pressure on the upper surface is increasing, while the under surface decreasing. This implies that Cl will decrease. The aerodynamic parameters including Cl and Cd changing along with AlphaT are shown as Figure 14.

Three influence regularities can be concluded from the trend of the curves and a numerical comparison:

a) Along with the thrust deflection angle changing from negative to positive, Cl decreases rapidly and linearly; and Cd decreases in a nonlinear way, too. These phenomena indicate that the thrust vector can generate intense supercirculation effects.

b) Cl and L/D ratio are $Cl = 0.403, K = 23.8$ when $AlphaT = 0^o$, while $Cl = 0.651, K = 35.6$ when $AlphaT = -7^o$. Compared to 0^o , Cl and L/D ratio are raised by $\eta_{Cl} = 61\%, \eta_K = 49.6\%$, which means the downward deflection of thrust can work as an actual flap, and improve the performance of a supercritical airfoil substantially.

c) The supercirculation induced by thrust vector can improve Cl and the L/D ratio simultaneously, which has a great potential to make a lift augmentation system. If the traditional augmentation system is replaced by supercirculation effects, the installment of traditional heavy components can be avoided, resulting in a higher flight performance.

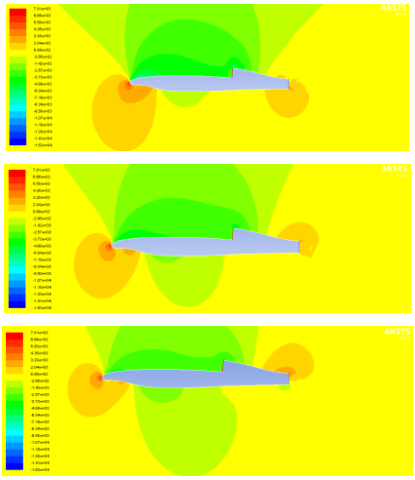

Figure 13 Pressure Nephograms of Thrust vector

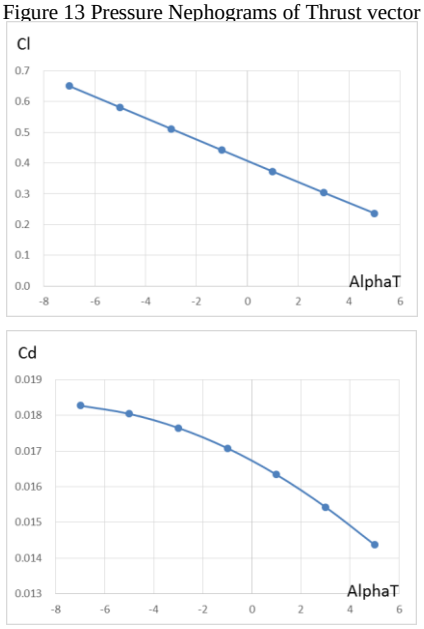

Figure 14 Aerodynamic Parameters of Basic Supercirculation

B. *Influence of BLI on supercirculation*

As described before, the supercirculation effects and BLI effects are the inseparable characteristics of DPC, thus the supercirculation effects affected by the BLI effects need to be studied.

The simulation results with different BLI intensities are shown as Figure 15.

Two influence regularities can be concluded from the distribution of curves and a numerical comparison:

a) The aerodynamic parameters under different BLI intensities appear to have the same trend, and the changing rate is almost the same along with AlphaT. This means the supercirculation effects are almost immune to BLI effects. To demonstrate this phenomenon more clearly, the aerodynamic parameters under the same AlphaT along with changing BLI intensity are shown as Figure 16.The high linearity of each curve and

the parallelity of different curves indicate that, under different AlphaT, the influence of BLI on aerodynamic parameters is in a same way. Synthesized results can be described like this: the influence of AlphaT and BLI can be linearly superimposed, which provides convenience for the use of supercirculation.

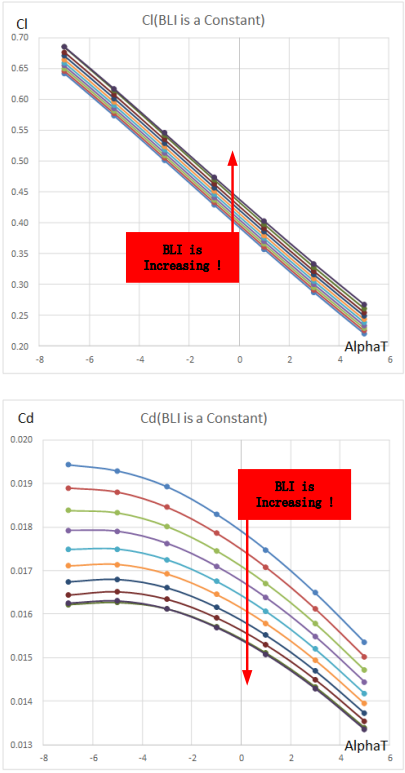

Figure 15 Aerodynamic Parameters Affected by BLI

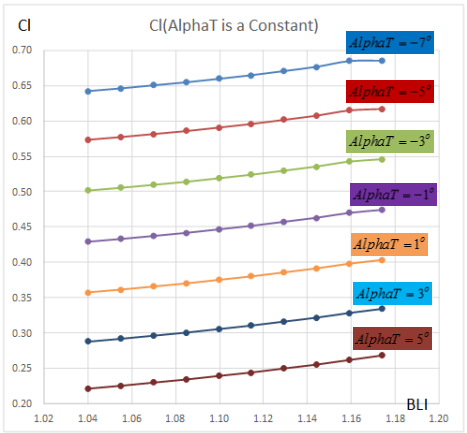

Figure 16 Aerodynamic Parameters under Different AlphaT

b) The specific research on BLI effects shows that BLI has the direct and effective influence on improving the flow field on the upper surface. The supercirculation effects can be regarded as to work on the basis of BLI effects. Only with the composition of these two features, the DPC can work most effectively.

C. Influence of jet velocity on supercirculation

Two elementary factors affecting the supercirculation effects include the thrust deflection angle and the jet velocity. The influence of jet velocity is discussed in this chapter, and the range of jet velocity is $V8 \in (266\,\text{m/s}, 299.2\,\text{m/s})$.

Under conditions of BLI intensity $\eta_{BLI} = 1.08$, $AOA = 0^o$ and $Ma = 0.6$, the aerodynamic parameters under different jet velocities $V8$ are shown as Figure 17:

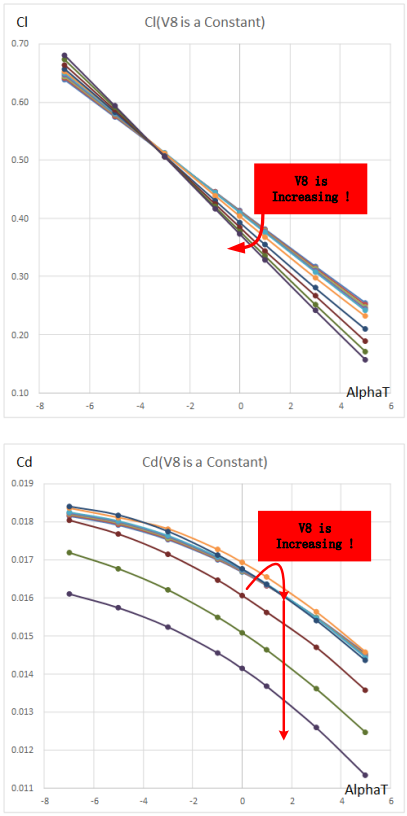

Figure 17 Aerodynamic Parameters Affected by V8

Four influence regularities can be concluded from the distribution of curves and a numerical comparison:

a) Even though the aerodynamic parameters appear to be in good linearity with AlphaT, but the influence of jet velocity on Cl appears to be nonlinear. Under -1^o, Cl will increase with the increasing of $V8$; but above -1^o, Cl will decrease with the increasing of $V8$. With a relatively higher jet velocity, the alternation of unit AlphaT on Cl and L/D ratio are larger, which means that a larger $V8$ can induce a stronger supercirculation.

b) With the upward deflecting of the thrust, Cd is decreasing. This is because the inducing effect on the under surface accelerates the flow velocity, and delays the flow separation, resulting in a reduced pressure drag. The trends of Cd under different jet velocities along with the AlphaT are almost the same, but under the same AlphaT, the influence of jet velocity appears to be nonlinear, as shown in Figure 18.When the jet velocity is relatively low, the influence of jet velocity on Cd is negligible. However, when the jet velocity is greater than 280m/s, Cd appears to increase firstly and then decrease, which is in accordance with the results of BLI's specific research.

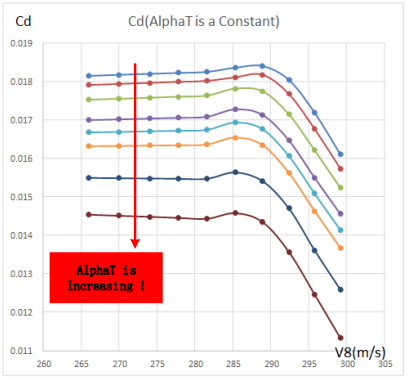

Figure 18 Influence of Jet Velocity on Cd

c) The maximal variation range of aerodynamic parameters caused by thrust vector are $\Delta Cl = 0.52$, $\Delta Cd = 0.0048$, $\Delta K = 28.4$ and the maximal range caused by jet velocity are $\Delta Cl = 0.098$, $\Delta Cd = 0.0032$, $\Delta K = 7$; the percentages of the above two situation are $\eta_{Cl} = 18.8\%$, $\eta_{Cd} = 66.7\%$, $\eta_K = 24.6\%$. Apparently, the influence of jet velocity is so strong that it cannot be neglected.

d) The jet velocity can affect the usable thrust directly, and the alternation of aerodynamic parameters caused by the change of jet velocity indicates that it will change the required thrust simultaneously. The relationship between the usable thrust and required thrust becomes quite complex with supercirculation. The nonlinearity and large extent of influence pose a great challenge on the application of supercirculation effects.

D. Influence of AOA on supercirculation

Under conditions of BLI intensity $\eta_{BLI} = 1.08$, jet velocity $V8 = 285.3m/s$ and $Ma = 0.6$, the aerodynamic parameters under different AOA are shown as Figure 19 and the range of AOA is $AOA \in [-2^o, 6^o]$.

Three influence regularities can be concluded from the distribution of curves and a numerical comparison:

a) Under conditions of different AOA, the influence of supercirculation effects on Cl is almost the same. Moreover, the supercirculation influence on Cl varies linearly along with AOA. It means that the supercirculation can still effectively work when there is AOA. The linearity and average distribution of curves indicate that the influence of AOA and basic supercirculation effects can be superimposed linearly. The variation range of Cl caused by basic supercirculation is $\Delta Cl = 0.45$, and the variation range of Cl caused by AOA variation is $\Delta Cl = 1.38$. The percentage of the former range divided by the latter one is $\eta_{Cl} = 32.6\%$, which means the supercirculation effects can be so strong that it will be revolutionized if well used.

b) When the AOA is relatively small, the slope of Cd is mild; but when the AOA is getting larger, the slope of Cd is getting steeper. This means the influence of supercirculation on Cd is getting stronger. The variation range of Cd is $\Delta Cd = 0.0039$ when $AOA = 0^o$, but $\Delta Cd = 0.05$ when $AOA = 6^o$, and it is 11.8 times larger than the previous one. This phenomenon indicates that the supercirculation effects can work more efficiently on drag reducing when AOA is larger. Cd varying along with the AOA is shown as Figure 20.

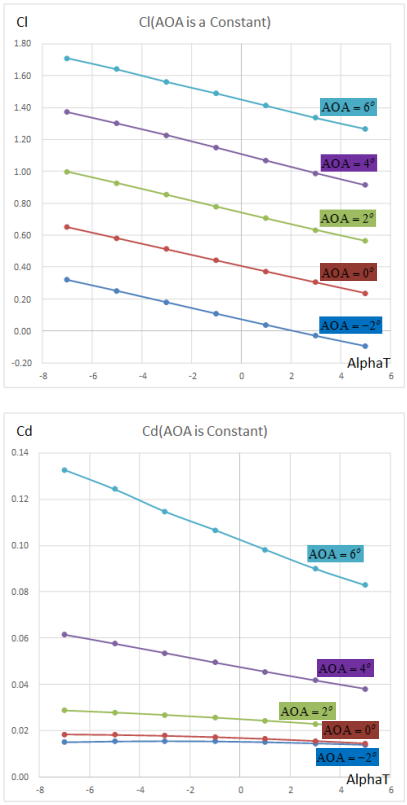

Figure 19 Aerodynamic Parameters Affected by AOA

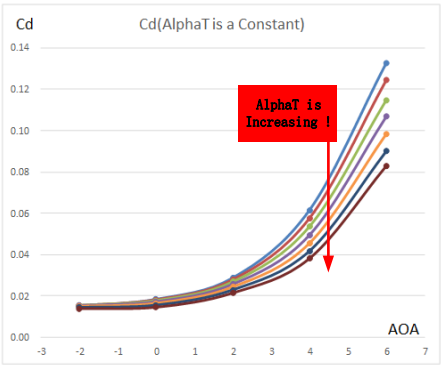

Figure 20 Cd Varying along with AOA

As can be seen, Cd increases rapidly when AOA is large sufficiently. If AOA can be suppressed under 2^o, L/D ratio will reach a relatively large one, while not raising the drag force apparently.

c) With the increasing of AOA, the L/D ratio curves generally move upward and then move downward, which is in accordance with the basic feature of AOA. A more intuitive illustration is shown as Figure 21.

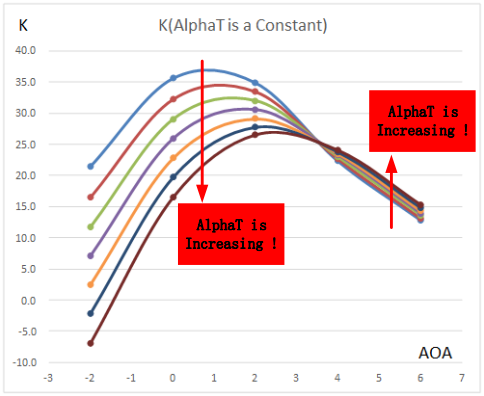

Figure 21 L/D ratio Varying along with AOA

E. Influence of flight speed on supercirculation

Under conditions of BLI intensity $\eta_{BLI}=1.08$, jet velocity $V8=285.3m/s$, $AOA=0^o$ and $Ma=0.8$, the aerodynamic parameters affected by thrust vector are shown as Figure 22:

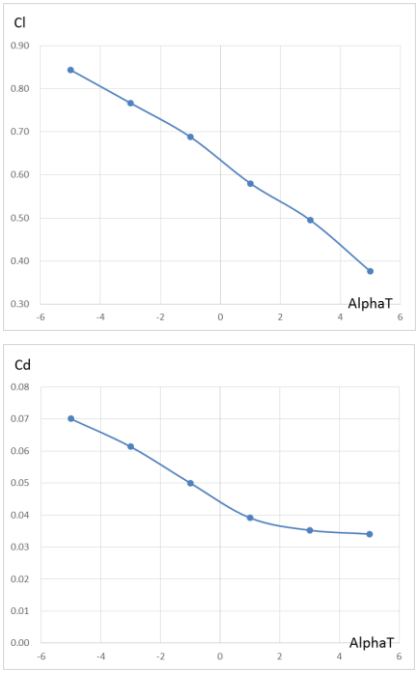

Figure 22 Aerodynamic Parameters Affected by Flight Speed

Three influence regularities can be concluded from the trend of curves and a numerical comparison:

a) When the flight speed is relatively high, the influence of supercirculation on aerodynamic parameters is still apparent;

b) Compared to $Ma=0.6$, Cd is generally larger. The variation range of aerodynamic parameters are $\Delta Cl=0.35,\Delta Cd=0.0037$ as $Ma=0.6$, and $\Delta Cl=0.47,\Delta Cd=0.036$ as $Ma=0.8$. These respectively are $\eta_{Cl}=1.34,\eta_{Cd}=9.7$ times larger than when $Ma=0.6$. As can be seen, when flight speed is high, the supercirculation effects are enhanced, especially on drag reducing. The reason is that due to the high flight speed, there emerges a local stall situation on the upper surface of airfoil, resulting in the strong wave drag. The upward deflection of thrust can effectively decrease the intensity of shock wave and reduce the wave drag, illustrated as Figure 23:

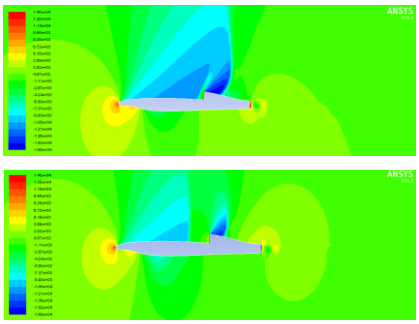

Figure 23 Pressure Nephograms with Shock Wave

c) Compare Cd curve of $Ma=0.6$ and $Ma=0.8$, the former curve's slope is getting larger along with the increasing of AlphaT, but the latter curve's slope is getting smaller. This is because the wave drag is the primary component of the current drag force. And with the upward deflection of thrust, the drag reducing effect on wave drag reaches a limitation.

V. Conclusion

Results show that the supercirculation effects have great potential to improve the flight performance, but due to the complexity of influence affected by multiple factors, it needs serious consideration and sophisticated design before application. The great advantage and high risk are always in company, which is the origin propelling power to urge a further research. The results in this paper form a solid foundation for the future work, and point out the most promising research directions.

Acknowledgment

Many Thanks for my adviser sincerely, who is a beautiful patient lady, and the most talented person I have ever met.

References

[1] Martin M. Dangelo GE Aviation, Lynn, Massachusetts John Gallman Vicki Johnson N+3 Small Commercial Efficient and Quiet Transportation for Year 2030-2035[R] NASA/CR–2010-216691

[2] Gregory S. Jones, William E. Miholen. Development of the Circulation Control Flow Scheme used in the NTF Semi-Span FAST-MAC Model[C]. Fluid Dynamics and Co-located Conferences, AIAA 2013-3048

[3] Gregory S. Jones. Pneumatic Flap Performance for a Two-Dimensional Circulation Control Airfoil [R] NASA Langley Research Center, AIAA 2005

[4] Francis J. Capone. Supercirculation Effects Induced by Vectoring a Partial-Span Rectangular Jet [J]. NASA Langley Research Center, J.AIRCRAFT, Vol 12, No 8, August 1975